ACS OMEGA

http://pubs.acs.org/journal/acsodf

Article

Tetrafluorophenylene-Containing Vinylbenzyl Ether-Terminated Oligo(2,6-dimethyl-1,4-phenylene ether) with Better Thermal, Dielectric, and Flame-Retardant Properties for Application in High-Frequency Communication

Yi-Chun Chen, Kamani Sudhir K. Reddy, Yu-An Lin, Meng-Wei Wang,* and Ching-Hsuan Lin*

Cite This: *ACS Omega* 2022, 7, 26396−26406

Read Online

ACCESS | Metrics & More | Article Recommendations | Supporting Information

ABSTRACT: In an integrated circuit, signal propagation loss is proportional to the frequency, dissipation factor (D_f), and square root of dielectric constant (D_k). The loss becomes obvious as we move to high-frequency communication. Therefore, a polymer having low D_k and D_f is critical for copper-clad laminates at higher frequencies. For this purpose, a 4-vinylbenzyl ether phenoxy-2,3,5,6-tetrafluorophenylene-terminated OPE (VT-OPE) resin was synthesized and its properties were compared with the thermoset of commercial OPE-2St resin. The thermoset of VT-OPE shows a higher T_g (242 *vs* 229 °C), a relatively high cross-linking density (1.59 *vs* 1.41 mmole cm^{-3}), a lower coefficient of thermal expansion (55 *vs* 76 ppm/°C), better dielectric characteristic at 10 GHz (D_k values of 2.58 *vs* 2.75, D_f values of 0.005 *vs* 0.006), lower water absorption (0.135 *vs* 0.312 wt %), and better flame retardancy (UL-94 VTM-0 *vs* VTM-1 with dropping seriously) than the thermoset of OPE-2St. To verify the practicability of VT-OPE for copper-clad laminate, a laboratory process was also performed to prepare a copper-clad laminate, which shows a high peeling strength with copper foil (5.5 lb/in), high thermal reliability with a solder dipping test at 288 °C (>600 s), and the time for delamination of the laminate in thermal mechanical analysis (TMA) at 288 °C is over 60 min.

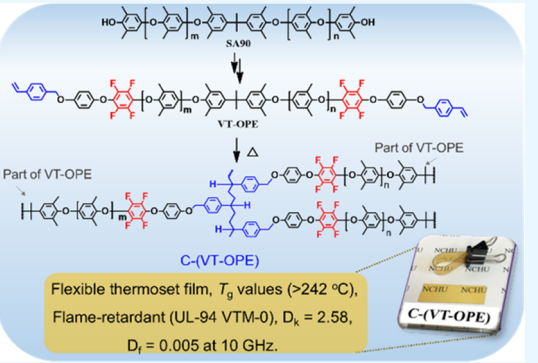

1. INTRODUCTION

In an integrated circuit, signal propagation speed (V_p) is inversely related to the square root of dielectric constant (D_k). The signal propagation loss (L) is directly related to the frequency, dissipation factor (D_f), and square root of the dielectric constant.[1]

$$V_p = C/\sqrt{D_k} \text{ and } L = K \times \left(\frac{f}{C}\right) \times D_f \times \sqrt{D_k} \quad (1)$$

In eq 1, C is a constant and f is the frequency. The propagation loss increases proportionally with the frequency. A polymer network with low D_k and D_f values can reduce the signal loss in high-frequency communication. In addition, a polymer network with a low D_k value can increase signal propagation speed. Many low-dielectric polymers have been reported in the literature.[2−19] Among them, poly(2,6-dimethyl-1,4-phenylene oxide) (PPO)[8,20−30] has been extensively studied due to its special characteristics such as low polarity, high T_g, low dielectric properties, and so forth. However, PPO also has some disadvantages, for example, properties like high melting point, limited solubility, and high viscosity, leading to their limited applications in copper-clad laminate industry.

To alleviate the shortcomings of PPO, oligo(2,6-dimethyl-1,4-phenylene ether) also known as OPE was established.[20−22,26,31−38] To compensate for the loss in thermal and mechanical properties owing to the low molecular weight of OPE, it should be cured with epoxy resins by terminal hydroxyl.[39] However, secondary hydroxyl groups with high polarity would be generated by the ring-opening reaction of epoxide, sacrificing the dielectric characteristic. To balance the dielectric and thermal properties, a typical commercial bifunctional OPE with end groups (vinylbenzyl ether) was developed by Mitsubishi Gas Chemical (MGC), named OPE-2St[40,41] (Figure 1). Using this resin, a self-cross-linking process could be achieved without creating polar groups, *via* radical initiated polymerization of vinyl groups. The makers are recommending these materials for high-frequency printed circuit boards because they have excellent thermal qualities without losing

Received: April 10, 2022
Accepted: July 11, 2022
Published: July 22, 2022

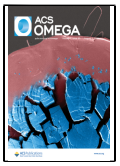

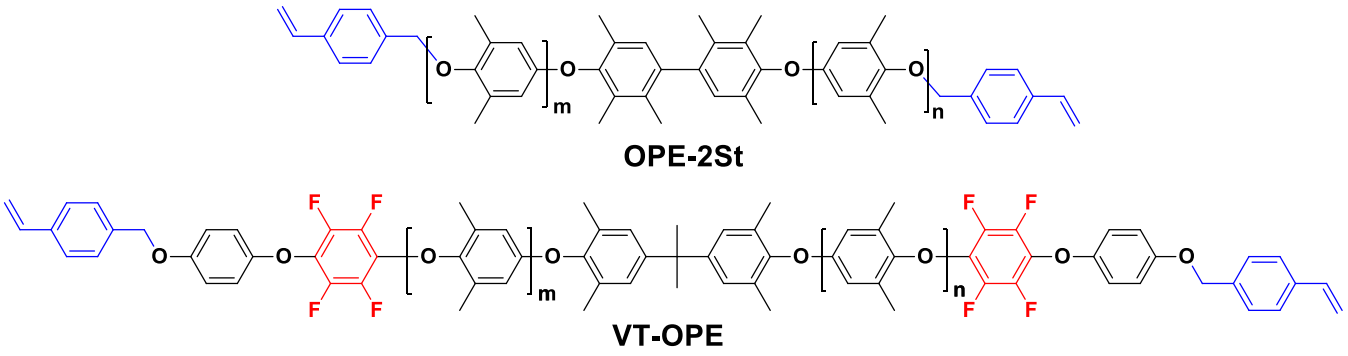

Figure 1. Structures of OPE-2St and VT-OPE.

Scheme 1. Attempted Synthesis of HT-OPE

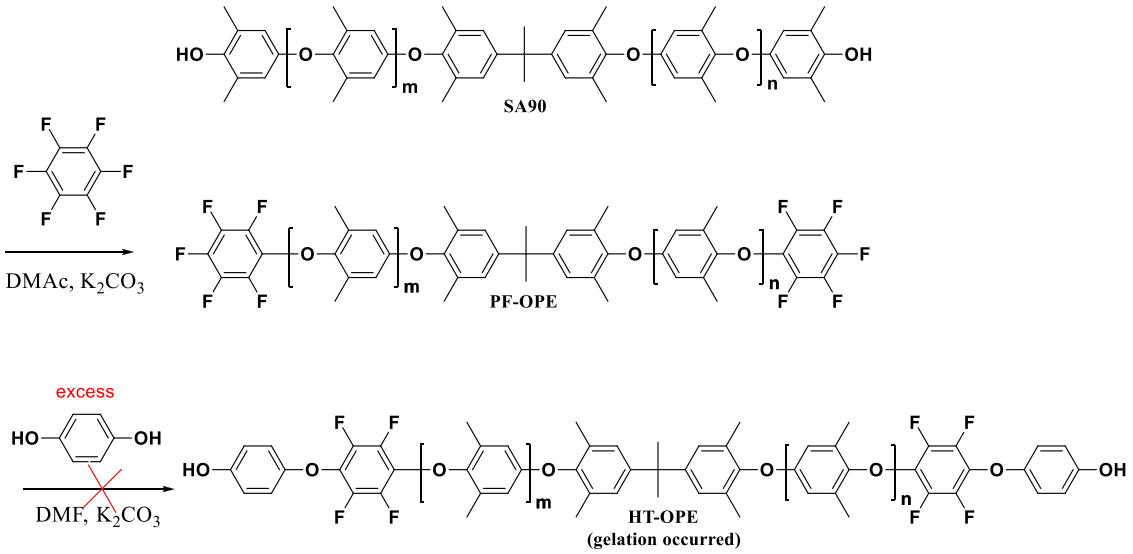

the necessary dielectric properties. However, one OPE-based material with all of the necessary features such as low dielectric constant, high glass-transition temperature, good dimensional stability, excellent thermal stability, minimal moisture absorption, high contact angle, and strong flame retardancy is rare.

It has been reported that incorporating fluoro-containing moieties can reduce the dielectric constant and enhance hydrophobicity.[3,5,42−57] Note that hydrophobicity is important for electronic materials since the D_k value of water is about 80 at room temperature, therefore moisture absorption of a thermoset has a negative effect on dielectric constant. Among the fluoro-containing moieties, we focus on the symmetric tetrafluorophenylene moiety that will not increase the dipole moment due to an equal distribution of polarizable C−F bonds. Therefore, our strategy is to incorporate the tetrafluorophenylene moieties at both ends to enhance the overall properties of OPE thermosets. For this purpose, a 4-vinylbenzyl ether phenoxy-2,3,5,6-tetrafluorophenylene-terminated OPE (VT-OPE) resin was first prepared. We found that cured VT-OPE (C-(VT-OPE)) shows better dielectric constant, hydrophobicity, and flame retardancy than the cured commercial resin OPE-2St (C-(OPE-2St)). Not only the detailed synthesis and curing behavior of VT-OPE resin but also the thermal, moisture absorption, and flame-retardant properties of the thermoset are discussed thoroughly. To verify the practicability of VT-OPE for copper-clad laminate, a process was performed to prepare a copper-clad laminate. Table S1 shows the overall performance data of different resins reported in the field of low-dielectric constant materials at high frequencies (in the GHz range).

2. EXPERIMENTAL SECTION

2.1. Materials. SA90 was purchased from SABIC (Saudi Basic Industries Corporation). Vinylbenzyl ether-terminated OPE named OPE-2St was purchased from MGC. *t*-Butyl cumyl peroxide (TBCP) was purchased from Sigma-Aldrich. Hexafluorobenzene and 4-benzyloxyphenol from Alfa Aesar, potassium carbonate from SHOWA, and 4-vinylbenzyl chloride and palladium on activated carbon (10% Pd/C) were purchased from Acros Organics. All of the solvents are of ACS or high-performance liquid chromatography (HPLC) grades.

2.2. Synthesis of OPEs. OPEs were synthesized according to the chemistries depicted in Schemes 1−3, and detailed synthetic procedures are shown below.

2.3. Synthesis of Pentafluorophenyl-Terminated Oligo(2,6-dimethyl-1,4-phenylene ether) (PF-OPE). SA90 (2.0 g, 1.25 mmol), hexafluorobenzene (1.16 g, 6.25 mmol), K_2CO_3 (0.43 g, 3.125 mmol), and DMAc (15 g) were added into a three-neck reactor equipped with a thermocouple, magnetic stirrer, and nitrogen flow. The solution was then kept for stirring at 80 °C for 36 h; after cooling to 25 °C, the crude suspension was poured into methanol/water (1/1, v/v), and the turbid solution was stirred overnight. The precipitate was filtered and dried in a vacuum oven for 12 h at 60 °C to get an off-white powder (yield = 86%). ^{1}H NMR (ppm, $CDCl_3$, 400

https://doi.org/10.1021/acsomega.2c02067
ACS Omega 2022, 7, 26396−26406

MHz): δ = 1.70 (6H, H^1), 2.09 (Ar−CH_3, H^3, H^5), 6.47 (Ar−H, H^4), and 6.97 (4H, H^2). ^{13}C NMR (ppm, $CDCl_3$, 100 MHz): δ = 16.77 (C^3, C^5), 30.95 (C^1), 114.40 (C^4), 127.35 (C^2), 135.61 (C^8), 137.24, 138.89 (C^6, C^{10}), 139.16, and 140.80 (C^7, C^9). ^{19}F NMR (ppm, $CDCl_3$, 376 MHz): δ = −159 (F at C^6, C^{10}), −157 (F at C^8), and −155 (F at C^7, C^9). Fourier transform infrared (FTIR) spectra (KBr, cm^{-1}): ν = 991 (C−F), 1197, 1308 (ether C−O), and 1606 (C═C). Gel permeation chromatography (GPC) (NMP): M_n = 3714 g/mol, and M_w = 5512 g/mol.

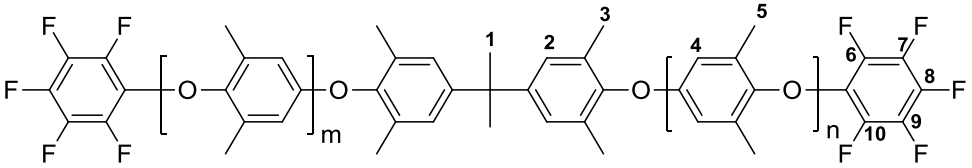

PF-OPE

2.4. Synthesis of 4-(Benzyl ether)phenoxy-2,3,5,6-tetrafluorophenylene-Terminated Oligo(2,6-dimethyl-1,4-phenylene ether) (BT-OPE). PF-OPE (1.0 g, 0.51 mmol), 4-benzyloxyphenol (0.2247 g, 1.122 mmol), K_2CO_3 (0.155 g, 1.122 mmol), and DMF (10 g) were taken into a 100 mL three-neck reactor equipped with a thermocouple, magnetic stirrer, and nitrogen flow. The solution was then kept for stirring for 12 h at 120 °C. After cooling to 25 °C, the reaction mixture was poured into methanol/water (1/1, v/v), and the turbid solution was stirred overnight. The precipitate was then filtered and dried in a vacuum oven for 12 h at 60 °C to get an off-white powder (yield = 85%). ^{1}H NMR (ppm, $CDCl_3$, 400 MHz): δ = 1.69 (6H, H^1), 2.08 (Ar−CH_3, H^3, H^5), 5.01 (4H, H^{12}), 6.46 (Ar−H, H^4), 6.89 (Ar−H, H^{10}, H^{11}, H^{15}), 6.97 (4H, H^2), and 7.39 (Ar−H, H^{13}, H^{14}). ^{13}C NMR (ppm, $CDCl_3$, 100 MHz): δ = 16.77 (C^3, C^5), 30.97 (C^1), 70.53 (C^{12}), 114.40 (C^4), 115.76 (C^{11}), 116.60 (C^{10}), 127.35 (C^2, C^{15}), 128.01 (C^{14}), and 128.58 (C^{13}). ^{19}F NMR (ppm, $CDCl_3$, 376 MHz): δ = −159 (F at C^6, C^{10}), and −155 (F at C^7, C^9). FTIR (KBr, cm^{-1}): ν = 991(C−F), 1191, 1302 (C−O−C), and 1601(Ar. C═C). GPC (NMP): M_n = 4587 g/mol, and M_w = 6132 g/mol.

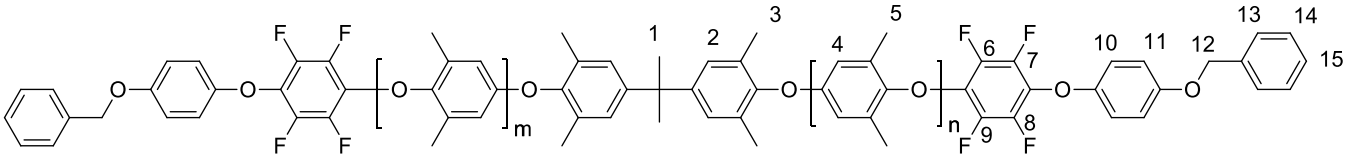

BT-OPE

2.5. Synthesis of 4-Hydroxylphenoxy-2,3,5,6-tetrafluorophenylene-Terminated Oligo(2,6-dimethyl-1,4-phenylene ether) (HT-OPE). BT-OPE (5.0 g, 2.15 mmol), Pd/C (0.25 g), and THF (50 mL) were taken in a 100 mL Parr reactor, equipped with a temperature sensor and hydrogen pressure regulator. The solution was stirred at 140 psi, for 24 h at 50 °C. After that, the reaction mixture was passed through Celite, and the filtrate was then poured into methanol/water (1/1, v/v). The precipitate was filtered and dried in a vacuum oven for 12 h at 60 °C to get a yellow powder (yield = 72%). ^{1}H NMR (ppm, $CDCl_3$, 400 MHz): δ = 1.70 (6H, H^1), 2.09 (Ar−CH_3, H^3, H^5), 5.30 (2H, OH), 6.48 (Ar−H, H^4), 6.89 (Ar−H, H^{10}, H^{11}), and 6.97 (4H, H^2). ^{13}C NMR (ppm, $CDCl_3$, 100 MHz): δ = 16.76 (C^3, C^5), 30.92 (C^1), 114.41 (C^4), 116.61 (C^{11}), 116.82 (C^{10}), and 127.36 (C^2). ^{19}F NMR (ppm, $CDCl_3$, 376 MHz): δ = −158 (F at C^6, C^{10}), and −154 (F at C^7, C^9). FTIR (KBr, cm^{-1}): ν = 991(C−F), 1191, 1308 (C−O−C), 1606 (Ar. C═C), and 3463 (−OH). GPC (NMP): M_n = 4225 g/mol, and M_w = 5404 g/mol.

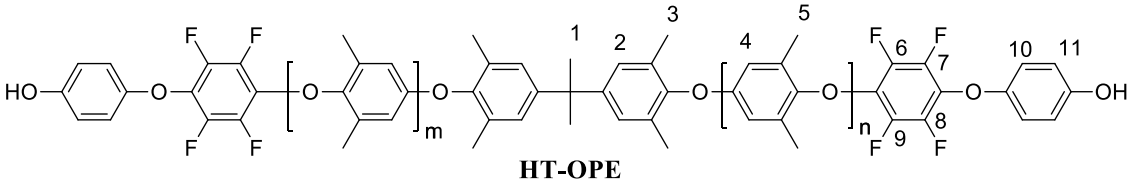

HT-OPE

2.6. Synthesis of 4-Vinylbenzyl Ether Phenoxy-2,3,5,6-tetrafluorophenylene-Terminated OPE (VT-OPE). HT-OPE (1.0 g, 0.4673 mmol), K_2CO_3 (0.3229 g, 2.337 mmol), 4-vinylbenzyl chloride (0.3922 g, 2.57 mmol), and DMAc (10 g) were taken in a 100 mL three-neck reactor equipped with a temperature sensor, nitrogen flow, and magnetic pellet. The solution was stirred at 100 °C for 24 h. After cooling to 25 °C, the reaction mixture was poured into methanol/water (1/1, v/v). The precipitate was filtered and dried in a vacuum oven for 12 h at 60 °C to get a white powder (yield = 82%). ^{1}H NMR (ppm, $CDCl_3$, 400 MHz): δ = 1.68 (6H, H^1), 2.08 (Ar−CH_3, H^3, H^5), 4.99 (4H, H^{12}), 5.25 (2H, H^{16}), 5.72 (2H, $H^{16'}$), 6.46 (Ar−H, H^4), 6.95(H^2, H^{10}, H^{11}, H^{15}), 7.34 (4H, H^{13}), and 7.40 (4H, H^{14}). ^{13}C NMR (ppm, $CDCl_3$, 100 MHz): δ = 16.77 (C^3, C^5), 31.03 (C^1), 70.30 (C^{12}), 114.41 (C^4), 115.79 (C^{11}), 116.61 (C^{10}), 126.40 (C^{14}), 127.36 (C^2), 127.64 (C^{13}), and 136.35 (C^{15}). ^{19}F NMR (ppm, $CDCl_3$, 376 MHz): δ = −159 (F at C^6, C^{10}), and −155 (F at C^7, C^9). FTIR (KBr, cm^{-1}): ν = 905 (C═C−H), 991 (C−F), 1191, 1302 (ether C−O), and 1601 (ar. C═C). GPC (NMP): M_n = 4069 g/mol, and M_w = 5194 g/mol.

https://doi.org/10.1021/acsomega.2c02067
ACS Omega 2022, 7, 26396−26406

Scheme 2. Synthesis of HT-OPE *via* Deprotection Procedure

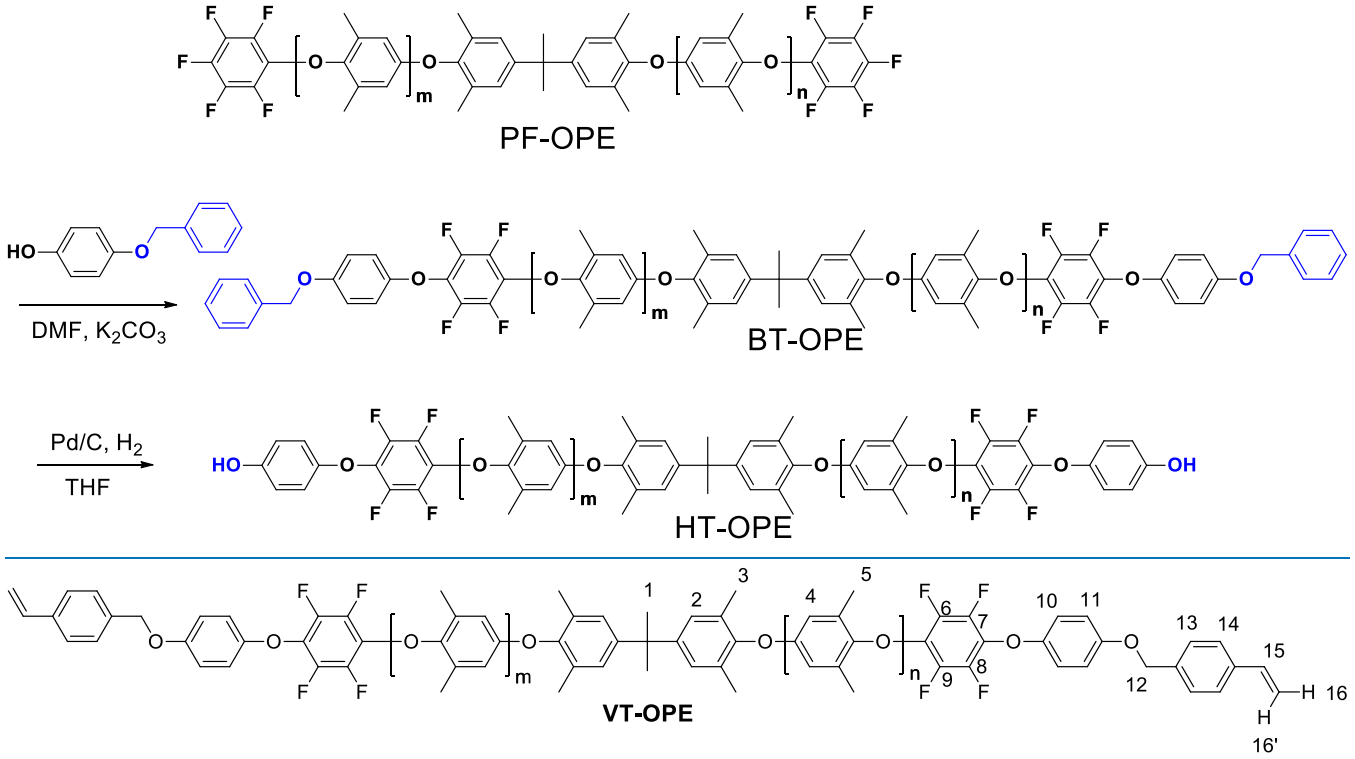

2.7. Thermosets Preparation *via* Self-Curing of OPEs. As shown in Scheme 4, self-cross-linking of vinyl groups of OPEs was performed using *tert*-butyl cumyl peroxide (TBCP) as an initiator to get the thermosets. The curing of VT-OPE exemplifies thermoset synthesis. VT-OPE (1.0 g) and TBCP (0.01 g) were dissolved in 4.04 g of xylenes (is commonly used solvent for the CCL industry) and taken in an aluminum mold. The solvent was kept for drying at 80 °C for 12 h and then cured at 120 °C (2 h), 180 °C (2 h), 200 °C (2 h), and 220 °C (2 h) under a nitrogen atmosphere. The thermosets of VT-OPE and OPE-2St are named as C-(VT-OPE) and C-(OPE-2St), respectively, where C refers to cured.

2.8. Preparation of Copper-Clad Laminate. VT-OPE was dissolved in toluene to make a solution with a solid content of 40 wt %. E-glass cloth (AST#106 L glass) was immersed in the solution for 30−50 s and subsequently dried at 70 °C for 10 min to prepare the prepreg. The copper-clad laminate was manufactured by stacking six pieces of prepregs with copper foil (18 μm) on each side. The heating and pressing process is 130 °C/15 min, 150 °C/0.15 MPa/15 min, 170 °C/0.45 MPa/30 min, 170 °C/0.75 MPa/1.5 h. The laminate was post-cured at 200 °C for 2 h to form a copper-clad laminate.

2.9. Characterization. NMR measurements: Varian Inova 400 NMR in DMSO-d_6 (or in $CDCl_3$).

Differential scanning calorimetry (DSC): PerkinElmer DSC 8000, the heating rate was 10 °C/min. Thermogravimetric analysis (TGA): PerkinElmer Pyris1 at a heating rate of 20 °C/min under a nitrogen atmosphere.

Dynamic mechanical analysis (DMA): PerkinElmer Pyris Diamond DMA, programmed heating rate of 5 °C/min with a frequency of 1 Hz. Storage modulus and tan δ were observed with respect to temperature.

Dielectric properties: Rhodes Schwarz vector network analyzer at 10 GHz, on the thin film with a dimension of 9 cm × 13 cm. The exact thickness of the film was measured for each test (5−100 μm).

Water absorption tests: The samples were dipped into boiling water for a few minutes (5 min), the gained weight was measured, and wettability was calculated using the formula $(W - W_0)/W_0 \times 100$ (%), where W is the weight of the sample after placing in water and W_0 is the weight of the sample before placing in water.

Thermal mechanical analysis (TMA): A SII TMA/SS6100 with a heating rate of 5 °C/min was used.

Gel permeation chromatography (GPC): A Hitachi-L2400 (NMP as solvent) gel permeation chromatogram was used at 40 °C with a flow rate of 1.0 mL/min. The instrument was calibrated using polystyrene as standards (M_n = 4130, 10 730, 200 000, and 300 000 g/mol).

Contact angle: The data were collected using an FTA1000B through the Sessile drop method using water as a testing liquid.

FTIR spectra: A PerkinElmer RX1 infrared spectrophotometer was used to scan the wavenumber ranging 400−4000 cm^{-1}.

Flame retardancy of the OPE thermosets was measured by a UL-94 VTM vertical thin-film test. In that test, an 8″ × 2″ sample was wrapped around a 1/2″ mandrel and then taped on one end. The mandrel was removed, leaving a cone-shaped sample that was relatively rigid. The two flame applications were applied, 3 s for each ignition to perform the UL-94 VTM vertical thin-film tests. After the first ignition, the flame was removed and the time for the polymer to self-extinguish (t_1) was recorded. Cotton ignition was noted if polymer dripping occurred during the test. After cooling, the second ignition was performed on the same sample and the self-extinguishing time (t_2) and dripping characteristics were recorded. If t_1 plus t_2 was less than 10 s without any dripping, the polymer was considered to be a VTM-0 material. If t_1 plus t_2 was in the range of 10−30 s without any dripping, the polymer was considered to be a VTM-1 material. In another scenario, if the material can self-extinguish in <10 s

https://doi.org/10.1021/acsomega.2c02067
ACS Omega 2022, 7, 26396−26406

Scheme 3. Synthesis of VT-OPE from HT-OPE

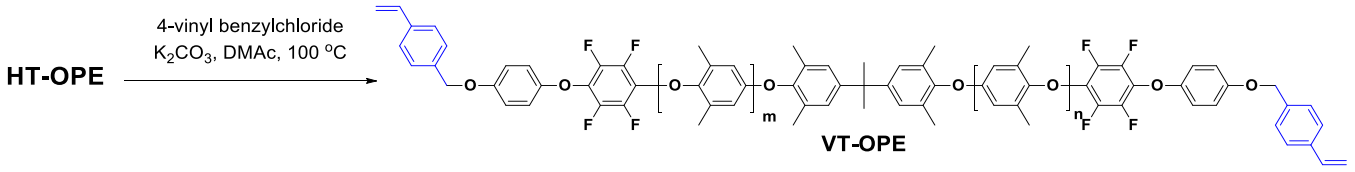

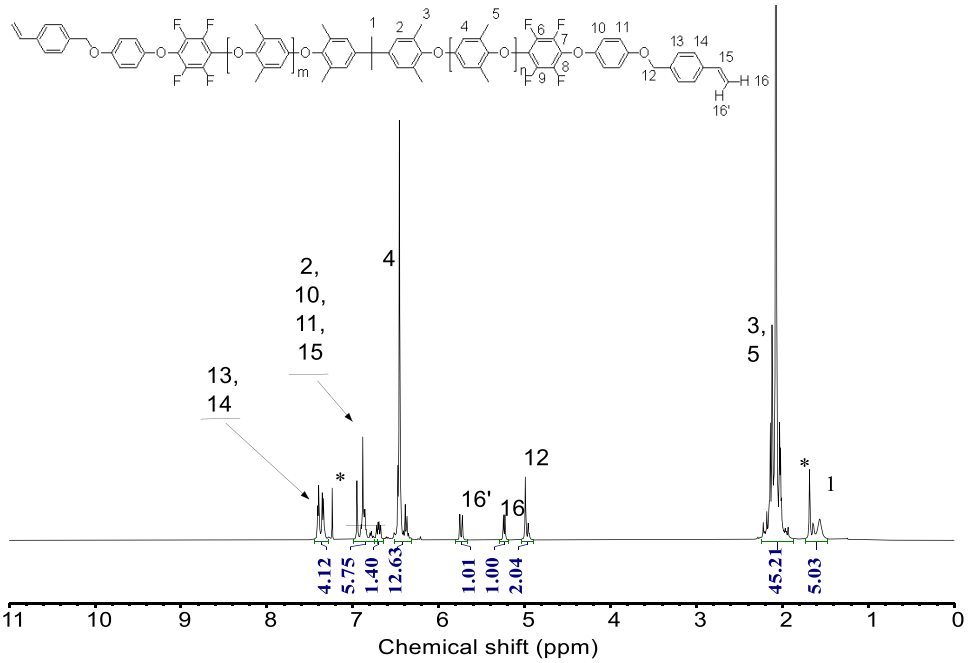

Figure 2. ^{1}H NMR spectrum of VT-OPE in $CDCl_3$, as per ^{1}H NMR the $m + n$ is approximately 6 pronouncing VT-OPE as an oligomer.

with dripping liquid surrounded by fire, then such material is considered as VTM-1 grade. Pressure cook test: A standard procedure to understand the reliability of CCL. The CCL is put in a pressured tank with water and heated to 120 °C for 2 h to absorb saturated water. After that, the CCL was put in a solder at 288 °C. The position of the CCL in the solder can be horizontal (floating test) or vertical (dipping test). If the CCL remains intact without delamination for 3 min, it is called "pass". In this work, the CCL based on VT-OPE can pass the solder floating test and the solder dipping test after the pressure cook test.

3. RESULTS AND DISCUSSION

3.1. Synthesis and Characterization of HT-OPE. The design of this work is to incorporate the symmetric tetrafluorophenylene moiety into OPEs to simultaneously enhance properties such as thermal, dielectric property, hydrophobicity, and flame retardancy. SA90 is a fully developed hydroxyl-terminated OPE from SABIC. It is suitable for preparing telechelic OPE derivatives through an elementary reaction, such as nucleophilic addition or nucleophilic substitution. Therefore, we proposed a synthetic route to prepare a fluoro-containing OPE with hydroxyl end groups (HT-OPE) using SA90 as a starting material (Scheme 1).

Firstly, PF-OPE was successfully prepared from SA90 with hexafluorobenzene at around 80 °C. When PF-OPE was further reacted with excess hydroquinone (about 4 equiv), gelation was observed (Scheme 1). It is probable that the pentafluorophenyl moieties of PF-OPE exhibited great reactivity, causing the undesirable polymerization or tri-substituted cross-link.[58] To obtain the critical precursor HT-OPE for further functionalization, a two-step synthetic strategy has been proposed in Scheme 2. PF-OPE reacted with 4-benzyloxyphenol at 120 °C to obtain BT-OPE in the first step. After deprotecting the benzyl group from hydroxyl of BT-OPE by catalytic (Pd/C) hydrogenation, we successfully received HT-OPE.

Figure S1 shows the ^{1}H NMR spectra of SA90, PF-OPE, BT-OPE, and HT-OPE in $CDCl_3$. In Figure S1a,b, the broad hydroxyl signal at 4.5 ppm in SA90 was not observed in PF-OPE, indicating that the reaction has already been completed. In Figure S1c, the Ar−H signals at 6.89−7.39 ppm and the methylene signal of benzyl ether (H^{12}) at 5.01 ppm support the formation of BT-OPE. For Figure S1d, the appearance of hydroxyl signal (H^{12}) at 5.30 ppm and the disappearance of methylene signal of benzyl ether support the formation of HT-OPE. Figure S2a shows the ^{19}F NMR spectra of PF-OPE; the characteristic −F atom bonded with C^8 is located at −157 ppm as a triplet with a lower intensity than the rest of the −F atom bonded with C^6, C^7, C^8, and C^9. In Figure S2b, the intensity of this triplet (−F at C^8) is negligible suggesting the presence of benzyloxyphenyl ether at −*para* position. Figure S3 shows the FTIR spectra of SA90, PF-OPE, BT-OPE, and HT-OPE. For Figure S3a,b, the disappearance of the hydroxyl signal at 3572 cm^{-1} and the appearance of the C−F bond at 991 cm^{-1} indicate PF-OPE formation. For Figure S3d, the hydroxyl signal at 3563 cm^{-1} and the C−F bond at 991 cm^{-1} indicate HT-OPE formation. Figure S4 shows the matrix-assisted laser desorption ionization−time-of-flight (MALDI-TOF) mass spectrum of HT-OPE. Various $m + n$ values corresponding to the HT-OPE

https://doi.org/10.1021/acsomega.2c02067
ACS Omega 2022, 7, 26396−26406

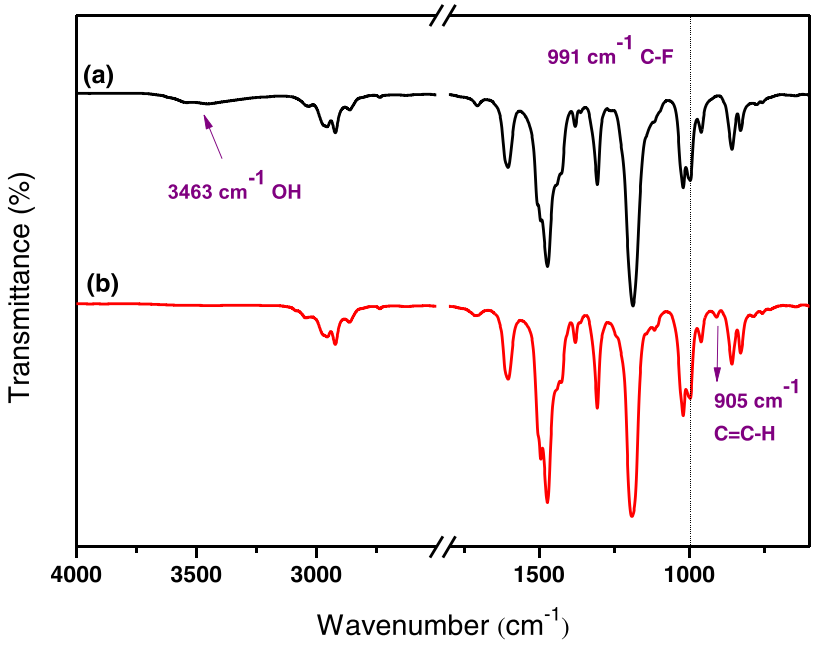

Figure 3. FTIR spectra of (a) HT-OPE and (b) VT-OPE.

Table 1. Solubility of SA90, VT-OPE, and OPE-2St

sample code	DMAc	DMF	NMP	THF	MEK	Toluene	$CHCl_3$	DCM	PM
SA90	++[a]	++	++	++	++	++	++	++	+−
VT-OPE	++	++	++	++	++	++	++	++	+h
OPE-2St	++	++	++	++	++	++	++	++	+−

[a]++, soluble at room temperature; +h, soluble on heating (80 °C); +−, slightly soluble on heating (80 °C). Solubility tests were conducted by taking 5 mg of sample in 2 mL of test solvent.

structure have been listed in the figure, further confirming the structure.

3.2. Synthesis of VT-OPE. As shown in Scheme 3, VT-OPE was prepared by reacting HT-OPE with 4-vinylbenzyl chloride in the presence of K_2CO_3. Figure 2 shows the ^1H NMR spectrum of VT-OPE in $CDCl_3$. We can see the characteristic signals at 5.3, 5.7 ppm for vinyl (H^{16} and $H^{16'}$) and 5.0 ppm for vinylbenzyl ether (H^{12}). Similarly, no characteristic signal of the hydroxyl group at 5.30 ppm was observed, indicating a complete nucleophilic substitution. Figure 3 displays the FTIR spectra of HT-OPE and VT-OPE. For VT-OPE, the appearance of a small vinyl peak at 905 cm^{-1} is also accompanied by the disappearance of hydroxyl. MALDI-TOF mass spectra of VT-OPE are provided in Figure S5, further confirming the individual structure.

3.3. GPC and Solubility Data of OPEs. GPC curves of (i) SA90, (ii) PF-OPE, (iii) BT-OPE, (iv) HT-OPE, and (v) VT-OPE are shown in Figure S6a, GPC curves of (i) blank NMP and (ii) OPE-2St are shown in Figure S6b. The molecular weights (M_n) of the OPE-based resins are between 3500 and 4500 g/mol with a PDI of 1.2−1.4 Đ. The M_n of VT-OPE is slightly lower than OPE-2St (with M_n = 4336 g/mol). Table 1 lists the solubility data of SA90, VT-OPE, and OPE-2St. Since the M_n values of all of the OPE-based resins are nearly similar, their solubility is also quite similar. The addition of the tetraphenylene moiety has no negative effect on the solubility of VT-OPE; therefore, we expect that VT-OPE would follow the same processing pattern as that of commercial OPE-2St so that it is convenient to produce commercial copper-clad laminates.

3.4. Curing Behavior of VT-OPE. Figure 4 shows DSC thermograms of VT-OPE with and without 1.0 wt % TBCP. For

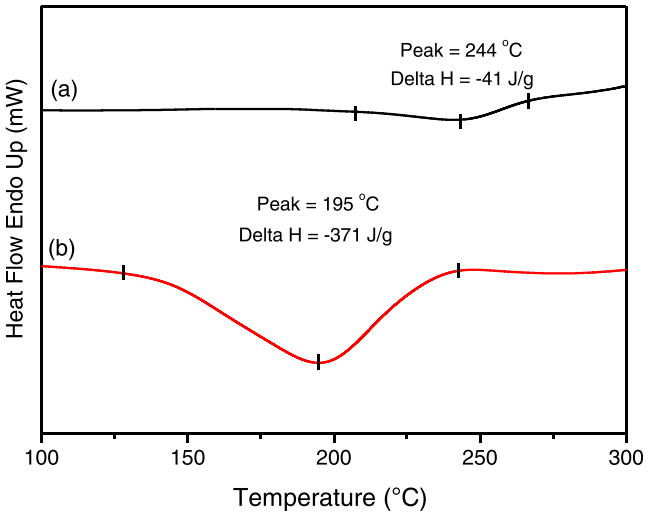

Figure 4. DSC thermograms of (a) neat VT-OPE and (b) VT-OPE with 1.0 wt % of TBCP.

Figure 4a, a non-notable exothermic characteristic of neat VT-OPE occurred at 244 °C. However, as shown in Figure 4b, a big exothermic peak temperature of VT-OPE with 1 wt % TBCP reduced remarkably to around 190 from 244 °C, and the corresponding exothermic enthalpy increased quite substan-

https://doi.org/10.1021/acsomega.2c02067
ACS Omega 2022, 7, 26396−26406

Scheme 4. Proposed Curing Chemistry of VT-OPE

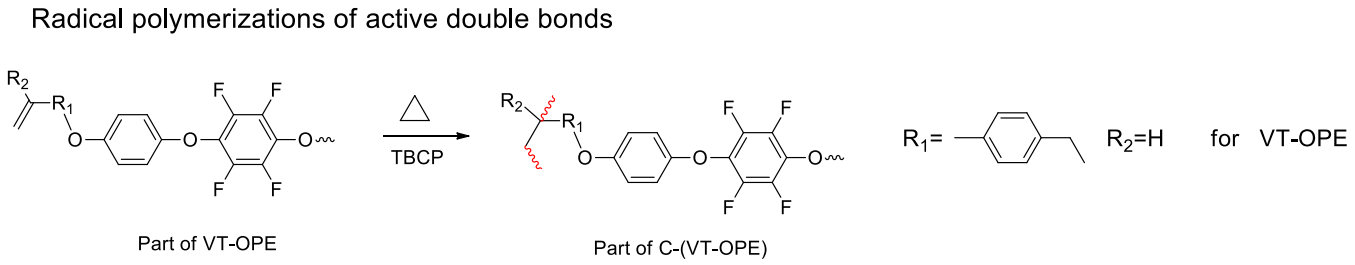

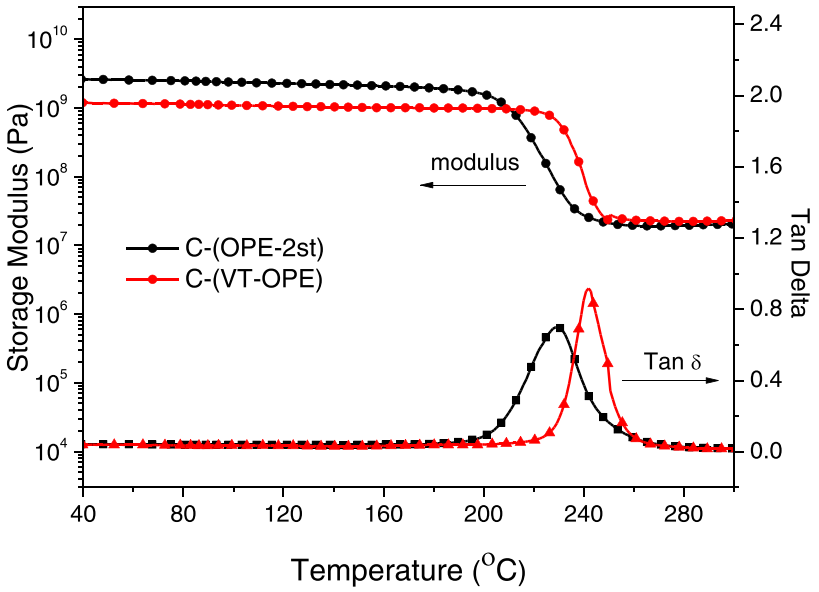

Figure 5. DMA thermograms of C-(VT-OPE) and C-(OPE-2St).

tially. Therefore, we suggest that the radical polymerization of vinylbenzene could be initiated successfully by TBCP between 150 and 220 °C, impelling us to use TBCP as an initiator to cure VT-OPE. To check the structures of thermosets, FTIR analyses were performed. Figure S7 shows the FTIR spectra of (a) VT-OPE and (b) C-(VT-OPE). For C-(VT-OPE), the disappearance of vinyl characteristic peak at 905 cm^{-1}, and the intensity reduction of the styrene $-CH{=}CH_2$ peak at 2932 cm^{-1} supports the radical polymerization of vinyl groups (Figure S7). Besides those mentioned above, there are no other remarkable variations in FTIR spectra. However, some literature has disclosed an unexpected curing chemistry of tetrafluorophenylene units. Kobrina et.al. reported that the reactions of hexafluorobenzene with alkyl radicals would generate the mixtures of fluoro-containing dimers (see Scheme 2 in ref 59). AlliedSignal, Inc. disclosed that bifunctional radicals from bistriazenes would cross-link with a fluorinated poly(arylene ether).[60] This type of chemistry was studied very less in the literature; to shed some light on it, we have verified the real possibility of an unexpected reaction (Scheme S1) of fluorinated moieties with radicals (from TBCP) by doing some model study. We have performed DSC thermograms on PF-OPE, BT-OPE, and HT-OPE with 1.0 wt % TBCP (Figure S8). As shown in Figure S8a, all of the tetrafluorophenylene moiety-containing samples showed exothermic peaks even though they do not contain any cross-linking unit (4-methyl styrene). To further explain the reason for the existence of the exothermic peak, we have tested DSC of TBCP alone (Figure S8a), and surprisingly, the exothermic peak is indeed caused by the dissociation of the TBCP, rather than the dimerization of tetrafluorophenylene moieties shown in Scheme S1. Figure S8b shows DSC thermograms of PF-OPE, BT-OPE, and HT-OPE without the addition of TBCP catalyst, and no exothermic peaks were observed in any of the samples. As a result, the proposed curing chemistry of VT-OPE is only radical polymerizations of active double bonds of styrene moieties (Scheme 4).

3.5. DMA and TMA Thermograms. Figure S9 shows the photograph of C-(VT-OPE); it can be folded without cracking. Figure 5 and Table 2 show the DMA thermograms and thermal data of C-(VT-OPE). Post T_g, stable modulus plateaus ($E' > 10^7$ Pa after T_g) were observed for both the samples, indicating that they belong to highly cross-linked network. The T_g value, defined by the peak maximum temperature of the tan δ curve, is 242 °C for C-(VT-OPE), which is 13 °C higher than the commercial C-(OPE-2St). The modulus at T_g +40 °C (the rubbery modulus) is 22 MPa for C-(VT-OPE), whereas the modulus at T_g +40 °C is 19 MPa for the commercial C-(OPE-2St). The cross-linking density, according to $E'/3RT$, in which E' is the storage modulus in the rubbery plateau,[61] is listed in Table 2.

Polymeric material with a low coefficient of thermal expansion (CTE) is essential to use in electronic applications. Figure S10 displays the TMA thermograms of C-(OPE-2St) and C-(VT-OPE). The T_g value (onset temperature of dimensional change), is 202 °C for C-(VT-OPE), which is 26 °C higher than that of C-(OPE-2St). The CTE value is 55 ppm/°C for C-(VT-OPE), which is much better than that of the C-(OPE-2St) (76 ppm/°C).

https://doi.org/10.1021/acsomega.2c02067
ACS Omega 2022, 7, 26396−26406

Table 2. Thermal Properties of C-(VT-OPE) and C-(OPE-2St)

sample code	T_g (°C) (DMA)[a]	E' at T_g +40 °C (MPa)	cross-linking density (mmole/cm^3)[b]	T_g (°C) (TMA)[c]	CTE (ppm/°C)[d]
C-(VT-OPE)[e]	242	22	1.59	202	55
C-(OPE-2St)[e]	229	19	1.41	199	76

[a]Measured by DMA at a heating rate of 5 °C/min. Defined by the peak temperature of the tan δ curve. [b]The cross-linking density accords with $E'/3RT$, in which E' is the storage modulus in the rubbery plateau (E' at T_g +40 °C). [c]Measured by TMA at a heating rate of 5 °C/min. Defined by the onset temperature of TMA thermograms. [d]Coefficient of thermal expansion, defined at 50 to 150 °C by TMA thermograms. [e]M_n of VT-OPE is 4069 g/mol, and M_n of OPE-2St is 4336 g/mol (NMP as the eluting solvent) the respective results are depicted in Figure S6a,b.

3.6. Thermal Stability and Flame Retardancy. Figure 6 and Table 3 display the TGA thermograms and data of C-(VT-OPE) and C-(OPE-2St). The decomposition temperatures $T_{d5\%}$ and $T_{d10\%}$ of C-(VT-OPE) are 420 and 455 °C, respectively, which are at least 25 °C higher than commercial C-(OPE-2St). The char yield is 38 wt % for C-(VT-OPE), which is 11 wt % higher than that of the commercial C-(OPE-2St). The enhanced char yield for C-(VT-OPE) can be ascribed to the higher cross-linking density, which can promote the carbon content, in other words char formation.[62,63] Table 3 also listed the flame-retardant data of C-(VT-OPE) and C-(OPE-2St). The sum of two burning times is 2.6 for C-(VT-OPE) without any fire dripping. Therefore, it belongs to UL-94 VTM-0 grade since the sum of the two burning times is less than 10 s and without any dripping. However, C-(OPE-2St) could not obtain VTM-0 quality because of severe fire dripping during the test.

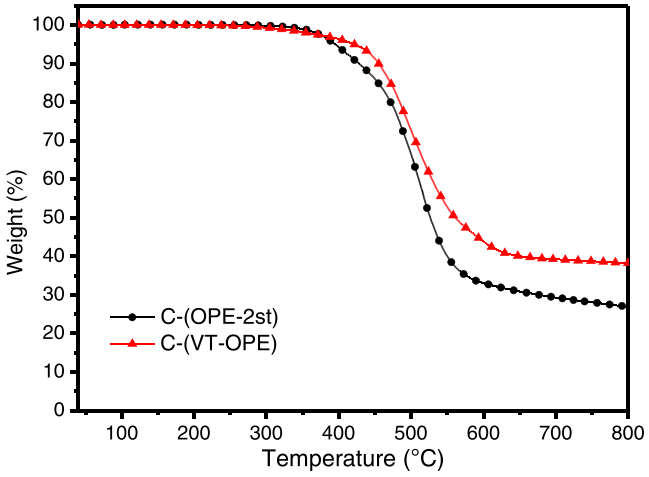

Figure 6. TGA thermograms of C-(VT-OPE) and C-(OPE-2St).

3.7. Water Absorption, Contact Angle, and Dielectric Properties. Hydrophobicity of polymeric material is as important as ultralow dielectric property for high-frequency transmission printed circuit boards. Moisture absorption of the polymeric material can have a negative impact on D_k. Table 4 lists the results of water absorption tests for C-(VT-OPE) and C-(OPE-2St). The saturated water absorption is around 0.135 wt % for C-(VT-OPE), whereas the saturated water absorption is about 0.312 wt % for C-(OPE-2St). Therefore, a 57% reduction in water absorption was observed through the incorporation of tetrafluorophenylene moiety. Figure S11 shows the contact angle of C-(VT-OPE) and C-(OPE-2St). The contact angles are 87 and 82° for C-(VT-OPE) and C-(OPE-2St), respectively, showing better hydrophobicity of the C-(VT-OPE). Table 4 also lists the dielectric properties of OPE thermosets. The D_k values are 2.58 and 2.75 for C-(VT-OPE) and C-(OPE-2St), respectively. A 6.2% reduction in the D_k value was observed. These dielectric results indicate the bulky tetrafluorophenylene moiety, which packs less densely and provides larger free volume, has an advantage in reducing the dielectric constant. We also hypothesize that the symmetric tetrafluorophenylene moiety can reduce polarizability within the chain because all of the electronegative fluorine atoms are distributed evenly and contribute to lower D_f characteristic.

3.8. Practicability of OPE Thermosets for Copper-Clad Laminate. The derivative CCLs were obtained by a simplified immersion process. The properties of CCL based on the VT-OPE are listed in Table 5. The properties of CCL based on OPE-2St are also presented to conduct a comparison. The CCL based on VT-OPE can pass the solder floating test and the solder dipping test after the pressure cook test at 120 °C for 2 h. No abrupt dimensional change was observed for the laminate in a TMA measurement at 288 °C, which means no delamination of the laminate during the test. It is worth noting that even incorporating fluoro-containing moieties, the CCL based on VT-OPE still exhibits good peeling strength with copper foil, which can be attributed to the relatively low fluorine content for VT-OPE compared with perfluorinated polymers. Additionally, the CCL based on VT-OPE shows a higher peeling strength with copper foil than OPE-2St. As a result, VT-OPE has the potential for application in high-frequency copper-clad laminates.

4. CONCLUSIONS

We have prepared a tetrafluorophenylene-containing vinylbenzyl ether-terminated oligo(2,6-dimethyl-1,4-phenylene ether) (VT-OPE) as a resin for copper-clad laminate to apply in high-frequency communication. The detailed structural investigation of VT-OPE resin and the thermal and mechanical properties of thermoset C-(VT-OPE) were discussed. C-(VT-OPE) thermoset shows a higher T_g (242 °C), a lower CTE (55 ppm/°C), a higher contact angle (87°), a lower dielectric constant (D_k = 2.58, D_f = 0.005 at 10 GH$_z$), and excellent flame-retardant property (VTM-0) compared to commercial C-(OPE-2St). These results demonstrate that incorporating the

Table 3. Thermal Stability and Flame-Retardant Properties of C-(VT-OPE) and C-(OPE-2St)

sample code	$T_{d5\%}$ (°C)[a]	$T_{d10\%}$ (°C)[b]	CY (%)[c]	1st burning time (s)	2nd burning time (s)	dripping	UL-94
C-(VT-OPE)	420	455	38	2.6	0	no	VTM-0
C-(OPE-2St)	394	427	27	3.3		seriously	VTM-1

[a]Temperature corresponds to 5% weight loss by thermogravimetry at a heating rate of 10 °C/min. [b]Temperature corresponds to 10% weight loss by thermogravimetry at a heating rate of 10 °C/min. [c]Char yield (residual weight % at 800 °C).

https://doi.org/10.1021/acsomega.2c02067
ACS Omega 2022, 7, 26396−26406

Table 4. Water Absorption, Contact Angle, and Dielectric Properties of C-(VT-OPE) and C-(OPE-2St)

	water absorption (%) at						
sample code	24 h	48 h	72 h	96 h	contact angle (°)	D_k (10 GHz)	D_f (10 GHz)
C-(VT-OPE)	0.135	0.135	0.135	0.135	87.0	2.58	0.005
C-(OPE-2St)	0.231	0.312	0.312	0.312	82.8	2.75	0.006

Table 5. Data of CCL Based on VT-OPE and OPE-2St

OPE for CCL	floating (s)[a]	peeling (lb/in)[b P]	dipping (s)[c]	TMA288 °C (min)[d]
VT-OPE	>600	5.5	>600	>60
OPE-2St	>600	4.7	>600	>60

[a]Time for the laminate to delaminate at solder floating test at 288 °C. [b P]eeling strength with copper foil (lb/in). [c]Time for the laminate to delaminate at solder dipping test at 288 °C after the laminate experience pressure cook test at 120 °C for 2 h. [d]Time for an abrupt dimensional change for the laminate in a TMA measurement at 288 °C, that is, the time for delamination of the laminate during the test.

tetrafluorophenylene moiety into OPE is a promising strategy to enhance the overall performance of the commercial C-(OPE-2St).

■ ASSOCIATED CONTENT

Supporting Information

The Supporting Information is available free of charge at https://pubs.acs.org/doi/10.1021/acsomega.2c02067.

NMR; GPC; MALDI-TOF; FTIR; thermomechanical properties; and contact angle data (PDF)

■ AUTHOR INFORMATION

Corresponding Authors

Meng-Wei Wang − *Advanced Material Development Department, Swancor High polymer Company Limited by Shares, Nantou 54066, Taiwan*; Email: stu00018@gmail.com

Ching-Hsuan Lin − *Department of Chemical Engineering, National Chung Hsing University, Taichung 40227, Taiwan*; orcid.org/0000-0003-0381-2736; Email: linch@nchu.edu.tw

Authors

Yi-Chun Chen − *Advanced Research Center for Green Materials Science and Technology, National Taiwan University, Taipei 10617, Taiwan*

Kamani Sudhir K. Reddy − *Department of Chemical Engineering, National Chung Hsing University, Taichung 40227, Taiwan*; orcid.org/0000-0001-7631-5517

Yu-An Lin − *Department of Chemical Engineering, National Chung Hsing University, Taichung 40227, Taiwan*

Complete contact information is available at: https://pubs.acs.org/10.1021/acsomega.2c02067

Author Contributions

Y.-C.C. performed laboratory experiments, analyzed the data, and wrote the first version of the manuscript. K.S.K.R. performed data analysis and wrote the second version of the manuscript. Y.-A.L. conducted laboratory experiments and data analysis. M.-W.W. teamed up with Y.-C.C. and K.S.K.R. for discussing the result and correcting the manuscript. C.H.L., principal investigator, contributed to idea conceptualization and guided the whole research team.

Notes

The authors declare no competing financial interest.

■ ACKNOWLEDGMENTS

This work was financially supported by the "Advanced Research Center For Green Materials Science and Technology" from The Featured Area Research Center Program within the framework of the Higher Education Sprout Project by the Ministry of Education (109L9006) and the Ministry of Science and Technology in Taiwan (MOST 109-2634-F-002-042 and 107-2221-E-005-025).

■ REFERENCES

(1) Maier, G. Low dielectric constant polymers for microelectronics. *Prog. Polym. Sci.* **2001**, *26*, 3−65.

(2) Chen, J.; Zeng, M.; Feng, Z.; Pang, T.; Huang, Y.; Xu, Q. Design and Preparation of Benzoxazine Resin with High-Frequency Low Dielectric Constants and Ultralow Dielectric Losses. *ACS Appl. Polym. Mater.* **2019**, *1*, 625−630.

(3) Kuo, C.-C.; Lin, Y.-C.; Chen, Y.-C.; Wu, P.-H.; Ando, S.; Ueda, M.; Chen, W.-C. Correlating the Molecular Structure of Polyimides with the Dielectric Constant and Dissipation Factor at a High Frequency of 10 GHz. *ACS Appl. Polym. Mater.* **2021**, *3*, 362−371.

(4) Zeng, M.; Chen, J.; Xu, Q.; Huang, Y.; Feng, Z.; Gu, Y. A facile method for the preparation of aliphatic main-chain benzoxazine copolymers with high-frequency low dielectric constants. *Polym. Chem.* **2018**, *9*, 2913−2925.

(5) Fang, L.; Zhou, J.; He, C.; Tao, Y.; Wang, C.; Dai, M.; Wang, H.; Sun, J.; Fang, Q. Understanding how intrinsic micro-pores affect the dielectric properties of polymers: an approach to synthesize ultra-low dielectric polymers with bulky tetrahedral units as cores. *Polym. Chem.* **2020**, *11*, 2674−2680.

(6) Liu, F.; Chen, X.; Fang, L.; Sun, J.; Fang, Q. An effective strategy for the preparation of intrinsic low-k and ultralow-loss dielectric polysiloxanes at high frequency by introducing trifluoromethyl groups into the polymers. *Polym. Chem.* **2020**, *11*, 6133−6170.

(7) Dai, M.; Tao, Y.; Fang, L.; Wang, C.; Sun, J.; Fang, Q. A Low Dielectric Polymer with High Thermostability Derived from Bio-based Vanillin. *ACS Sustainable Chem. Eng.* **2020**, *8*, 15013−15019.

(8) Wang, Y.; Tao, Y.; Zhou, J.; Sun, J.; Fang, Q. Biobased Anethole-Functionalized Poly(phenylene oxides): New Low Dielectric Materials with High Tg and Good Dimensional Stability. *ACS Sustainable Chem. Eng.* **2018**, *6*, 9277−9282.

(9) Qian, C.; Bei, R.; Zhu, T.; Zheng, W.; Liu, S.; Chi, Z.; Aldred, M. P.; Chen, X.; Zhang, Y.; Xu, J. Facile Strategy for Intrinsic Low-k Dielectric Polymers: Molecular Design Based on Secondary Relaxation Behavior. *Macromolecules* **2019**, *52*, 4601−4609.

(10) Wang, J.; Zhou, J.; Jin, K.; Wang, L.; Sun, J.; Fang, Q. A New Fluorinated Polysiloxane with Good Optical Properties and Low Dielectric Constant at High Frequency Based on Easily Available Tetraethoxysilane (TEOS). *Macromolecules* **2017**, *50*, 9394−9402.

(11) Lv, P.; Dong, Z.; Dai, X.; Qiu, X. Flexible Polydimethylsiloxane-Based Porous Polyimide Films with an Ultralow Dielectric Constant and Remarkable Water Resistance. *ACS Appl. Polym. Mater.* **2019**, *1*, 2597−2605.

(12) Chen, Z.; Zhu, D.; Tong, F.; Lu, X.; Lu, Q. Low Dielectric Constant Polyimide Hybrid Films Prepared by in Situ Blow-Balloon Method. *ACS Appl. Polym. Mater.* **2019**, *1*, 2189−2196.

(13) Li, X.; Liu, T.; Jiao, Y.; Dong, J.; Gan, F.; Zhao, X.; Zhang, Q. Novel high-performance poly(benzoxazole-co-imide) resins with low

https://doi.org/10.1021/acsomega.2c02067
ACS Omega 2022, 7, 26396−26406

dielectric constants and superior thermal stabilities derived from thermal rearrangement of ortho-hydroxy polyimide oligomers. *Chem. Eng. J.* **2019**, *359*, 641−651.
(14) Wang, L.; Liu, X.; Liu, C.; Zhou, X.; Liu, C.; Cheng, M.; Wei, R.; Liu, X. Ultralow dielectric constant polyarylene ether nitrile foam with excellent mechanical properties. *Chem. Eng. J.* **2020**, *384*, No. 123231.
(15) Wang, S.; Wang, L.; Wang, B.; Su, H.; Fan, W.; Jing, X. Facile preparation of recyclable cyclic polyolefin/polystyrene vitrimers with low dielectric loss based on semi-interpenetrating polymer networks for high-frequency copper-clad laminates. *Polymer* **2021**, *233*, No. 124214.
(16) Kourakata, Y.; Onodera, T.; Kasai, H.; Jinnai, H.; Oikawa, H. Ultra-low dielectric properties of porous polyimide thin films fabricated by using the two kinds of templates with different particle sizes. *Polymer* **2021**, *212*, No. 123115.
(17) Lu, H.; Li, D.; Zhang, Y.; Wu, Z.; Wang, H.; Liu, S.; Yan, G.; Yang, J.; Zhang, G. Design of low dielectric constant and high transparent polyarylate containing spiral ring. *Polymer* **2021**, *228*, No. 123948.
(18) Wang, Z.; Zhang, M.; Han, E.; Niu, H.; Wu, D. Structure-property relationship of low dielectric constant polyimide fibers containing fluorine groups. *Polymer* **2020**, *206*, No. 122884.
(19) Zhao, H.; Zhao, S.-Q.; Li, Q.; Khan, M. R.; Liu, Y.; Lu, P.; Huang, C.-X.; Huang, L.-J.; Jiang, T. Fabrication and properties of waterborne thermoplastic polyurethane nanocomposite enhanced by the POSS with low dielectric constants. *Polymer* **2020**, *209*, No. 122992.
(20) Chen, C. H.; Gu, Z. C.; Tsai, Y. L.; Jeng, R. J.; Lin, C. H. Identification of the reaction mechanism between phenyl methacrylate and epoxy and its application in preparing low-dielectric epoxy thermosets with flexibility. *Polymer* **2018**, *140*, 225−232.
(21) Chen, C.-H.; Lee, K.-W.; Lin, C.-H.; Juang, T.-Y. Low-Dissipation Thermosets Derived from Oligo(2,6-Dimethyl Phenylene Oxide)-Containing Benzoxazines. *Polymers* **2018**, *10*, No. 411.
(22) Chen, C.-H.; Liu, C.-H.; Ariraman, M.; Lin, C.-H.; Juang, T.-Y. Phosphinated Poly(aryl ether)s with Acetic/Phenyl Methacrylic/Vinylbenzyl Ether Moieties for High-Tg and Low-Dielectric Thermosets. *ACS Omega* **2018**, *3*, 6031−6038.
(23) Lin, Y.-C.; Chiang, C.-H.; Kuo, C.-C.; Hsu, S.-N.; Higashihara, T.; Ueda, M.; Chen, W.-C. A compatible and crosslinked poly(2-allyl-6-methylphenol-co-2,6-dimethylphenol)/polystyrene blend for insulating adhesive film at high frequency. *J Appl. Polym. Sci.* **2019**, *136*, No. 47828.
(24) Golla, M.; Nagendra, B.; Rizzo, P.; Daniel, C.; de Ballesteros, O. R.; Guerra, G. Polymorphism of Poly(2,6-dimethyl-1,4-phenylene)-oxide in Axially Stretched Films. *Macromolecules* **2020**, *53*, 2287−2294.
(25) Huang, Y.; Liu, W.; Jiang, Q.; Wei, Y.; Qiu, Y. Interlaminar Fracture Toughness of Carbon-Fiber-Reinforced Epoxy Composites Toughened by Poly(phenylene oxide) Particles. *ACS Appl. Polym. Mater.* **2020**, *2*, 3114−3121.
(26) Yang, J.; Jiang, H.; Gao, L.; Wang, J.; Ye, N.; Xu, Y.; He, R. Formation and investigation of dual cross-linked high temperature proton exchange membranes based on vinylimidazolium-functionalized poly(2,6-dimethyl-1,4-phenylene oxide) and polystyrene. *Polym. Chem.* **2018**, *9*, 5462−5469.
(27) Ingratta, M.; Elomaa, M.; Jannasch, P. Grafting poly(phenylene oxide) with poly(vinylphosphonic acid) for fuel cell membranes. *Polym. Chem.* **2010**, *1*, 739−746.
(28) Liang, M.; Jhuang, Y.-J.; Zhang, C.-F.; Tsai, W.-J.; Feng, H.-C. Synthesis and characterization of poly(phenylene oxide) graft copolymers by atom transfer radical polymerizations. *Eur. Polym. J.* **2009**, *45*, 2348−2357.
(29) Fukuhara, T.; Shibasaki, Y.; Ando, S.; Ueda, M. Synthesis of thermosetting poly(phenylene ether) containing allyl groups. *Polymer* **2004**, *45*, 843−847.
(30) Lee, T.-J.; Fang, Y.-D.; Yuan, W.-G.; Wei, K.-M.; Liang, M. Synthesis, structures and thermal properties of new class epoxide-terminated telechelic poly (2, 6-dimethyl-1, 4-phenylene oxide)s. *Polymer* **2007**, *48*, 734−742.
(31) Mei, W.; Wang, Z.; Yan, J. Poly(ether sulfone) copolymers containing densely quaternized oligo(2, 6-dimethyl-1, 4-phenylene oxide) moieties as anion exchange membranes. *Polymer* **2017**, *125*, 265−275.
(32) Chen, C. H.; Jheng, J. K.; Juang, T. Y.; Abu-Omar, M. M.; Lin, C. H. Structure-property relationship of vinyl-terminated oligo(2,6-dimethyl-1,4-phenylene ether)s (OPEs): Seeking an OPE with better properties. *Eur. Polym. J.* **2019**, *117*, 94−104.
(33) Tada, Y.; Moriya, N.; Kanazawa, M.; Asanuma, K.; Suzuki, A.; Koyama, S. Preparation and properties of novel oligo(phenylene oxide)-branched cyclophosphazenes. *Polym. Chem.* **2012**, *3*, 2815−2824.
(34) Chen, C.-W.; Lin, I. H.; Lin, C.-C.; Lin, J.-L.; Horie, M. Synthesis of poly(2,6-dimethyl-1,4-phenylene oxide) derivatives in water using water-soluble copper complex catalyst with natural ligands. *Polymer* **2013**, *54*, 5684−5690.
(35) Luo, L.; Qiu, T.; Meng, Y.; Guo, L.; Yang, J.; Li, Z.; Cao, X.; Li, X. A novel fluoro-terminated hyperbranched poly(phenylene oxide) (FHPPO): synthesis, characterization, and application in low-k epoxy materials. *RSC Adv.* **2013**, *3*, 14509−14520.
(36) Su, C.-T.; Lin, K.-Y.; Lee, T.-J.; Liang, M. Preparation, characterization and curing properties of epoxy-terminated poly-(alkyl-phenylene oxide)s. *Eur. Polym. J.* **2010**, *46*, 1488−1497.
(37) Yang, M. C.; Higashihara, T.; Su, H. W.; Ueda, M.; Chen, W.-C. Crosslinked copolymer with low dielectric constant and dissipation factor based on poly(2,6-Dimethylphenol-co−2,6-Diphenylphenol) and a crosslinker. *J. Polym. Sci., Part A: Polym. Chem.* **2016**, *54*, 3218−3223.
(38) Sakaguchi, Y.; Kitamura, K.; Yamashita, M.; Takase, S.; Takasugi, K.; Akitomo, Y. Synthesis and Properties of Sulfonated Poly(arylene ether)s with Flexible Oligomeric Phenylene Ether Segments. *Macromolecules* **2012**, *45*, 5403−5409.
(39) Peters, E. N. Hardener Composition. US20200270393A12018.
(40) Ohno, K. I. D. Curable Resin Composition, Curable Film and their Cured Products. US20080300350A12008.
(41) Ishii, K.; Norisue, Y.; Ohno, D.; Miyamoto, M. US6995195B22006.
(42) Han, D. J.; Kim, S.; Heo, H. J.; Park, I. J.; Kang, H. S.; Lee, S. G.; Lee, J.-C.; Sohn, E.-H. Access to Fluorinated Polymer Surfaces with Outstanding Mechanical Property, High Optical Transparency, and Low Surface Energy via Nonafluoro-tert-Butyl Group Introduction. *ACS Appl. Polym. Mater.* **2020**, *2*, 3957−3965.
(43) Luo, G.; Wen, L.; Yang, K.; Li, X.; Xu, S.; Pi, P.; Wen, X. Robust and durable fluorinated 8-MAPOSS-based superamphiphobic fabrics with buoyancy boost and drag reduction. *Chem. Eng. J.* **2020**, *383*, No. 123125.
(44) Velez-Herrera, P.; Doyama, K.; Abe, H.; Ishida, H. Synthesis and Characterization of Highly Fluorinated Polymer with the Benzoxazine Moiety in the Main Chain. *Macromolecules* **2008**, *41*, 9704−9714.
(45) Zhang, K.; Han, L.; Froimowicz, P.; Ishida, H. A Smart Latent Catalyst Containing o-Trifluoroacetamide Functional Benzoxazine: Precursor for Low Temperature Formation of Very High Performance Polybenzoxazole with Low Dielectric Constant and High Thermal Stability. *Macromolecules* **2017**, *50*, 6552−6560.
(46) Wu, J.; Xi, Y.; McCandless, G. T.; Xie, Y.; Menon, R.; Patel, Y.; Yang, D. J.; Iacono, S. T.; Novak, B. M. Synthesis and Characterization of Partially Fluorinated Polybenzoxazine Resins Utilizing Octafluorocyclopentene as a Versatile Building Block. *Macromolecules* **2015**, *48*, 6087−6095.
(47) Yin, X.; Feng, Y.; Zhao, Q.; Li, Y.; Li, S.; Dong, H.; Hu, W.; Feng, W. Highly transparent, strong, and flexible fluorographene/fluorinated polyimide nanocomposite films with low dielectric constant. *J. Mater. Chem. C* **2018**, *6*, 6378−6384.
(48) Chen, T.-B.; Li, Q.-N.; Liu, C.; Hong, R.; Li, Q.; Zhu, L.; Xu, C. Hydrophobic fluorinated colloidal photonic crystals for heterogeneous aggregated cluster encoding and energy-saving applications. *Chem. Eng. J.* **2021**, *411*, No. 128623.
(49) Fang, L.; Zhou, J.; Tao, Y.; Wang, Y.; Chen, X.; Chen, X.; Hou, J.; Sun, J.; Fang, Q. Low Dielectric Fluorinated Polynorbornene with Good Thermostability and Transparency Derived from a Biobased

https://doi.org/10.1021/acsomega.2c02067
ACS Omega 2022, 7, 26396−26406

Allylphenol (Eugenol). *ACS Sustainable Chem. Eng.* **2019**, *7*, 4078−4086.
(50) Shao, J.; Sheng, W.; Wang, C.; Ye, Y. Solvent-free fabrication of tough self-crosslinkable short-fluorinated copolymer nanocoatings for ultradurable superhydrophobic fabrics. *Chem. Eng. J.* **2021**, *416*, No. 128043.
(51) Chen, C. H.; Lin, C. H.; Wang, M. W.; Juang, T. Y. Low Dielectric Polyetherimides Derived from Bis[4-(4-(4-aminophenoxy)-2-tert-butylphenoxy)phenyl] Sulfone and 4,4′-Bis[4-(4-aminophenoxy)-2-tert-butylphenoxy]perfluorobiphenyl. *ACS Omega* **2017**, *2*, 4800−4807.
(52) Wu, M.; Xu, J.; Bai, S.; Chen, X.; Yu, X.; Naito, K.; Zhang, Z.; Zhang, Q. A high-performance functional phthalonitrile resin with a low melting point and a low dielectric constant. *Soft Matter* **2020**, *16*, 1888−1896.
(53) Fu, K.; Lu, C.; Liu, Y.; Zhang, H.; Zhang, B.; Zhang, H.; Zhou, F.; Zhang, Q.; Zhu, B. Mechanically robust, self-healing superhydrophobic anti-icing coatings based on a novel fluorinated polyurethane synthesized by a two-step thiol click reaction. *Chem. Eng. J.* **2021**, *404*, No. 127110.
(54) Wu, J.; Wang, C.; Lin, W.; Ngai, T. A facile and effective approach for the synthesis of fluorinated waterborne polyurethanes with good hydrophobicity and antifouling properties. *Prog. Org. Coat.* **2021**, *159*, No. 106405.
(55) Wang, X.; Cui, Y.; Wang, Y.; Ban, T.; Zhang, Y.; Zhang, J.; Zhu, X. Preparation and characteristics of crosslinked fluorinated acrylate modified waterborne polyurethane for metal protection coating. *Prog. Org. Coat.* **2021**, *158*, No. 106371.
(56) Godleman, J.; Leroux, F.; Reynolds, S.; Philpott, J.; Cranwell, P. B.; Harries, J. L.; Hayes, W.; Colquhoun, H. M. Aromatic poly (fluorocarbinol)s: Soluble, hydrophobic binders for inkjet formulations. *Prog. Org. Coat.* **2021**, *158*, No. 106378.
(57) Doss, J. R.; Shanahan, M. H.; Wohl, C. J.; Connell, J. W. Synthesis, characterization and evaluation of urethane co-oligomers containing pendant fluoroalkyl ether groups. *Prog. Org. Coat.* **2016**, *95*, 72−78.
(58) Irvin, J. A.; Neef, C. J.; Kane, K. M.; Cassidy, P. E.; Tullos, G.; St Clair, A. K. Polyethers derived from bisphenols and highly fluorinated aromatics. *J. Polym. Sci., Part A: Polym. Chem.* **1992**, *30*, 1675−1679.
(59) Kobrina, L. S. Some peculiarities of radical reactions of polyfluoroaromatic compounds. *J. Fluorine Chem.* **1989**, *42*, 301−344.
(60) Mercer, F. W.; Goodman, T. D.; Lau, A. N. K.; Vo, L. P. Crosslinkable Fluorinated Polyarylene Ether Composition. US5155175A,1990.
(61) Ariraman, M.; Sasikumar, R.; Alagar, M. Shape memory effect on the formation of oxazoline and triazine rings of BCC/DGEBA copolymer. *RSC Adv.* **2015**, *5*, 69720−69727.
(62) Wang, M. W.; Jeng, R. J.; Lin, C. H. The robustness of a thermoset of a main-chain type polybenzoxazine precursor prepared through a strategy of A−A and B−B polycondensation. *RSC Adv.* **2016**, *6*, 18678−18684.
(63) Agag, T.; Takeichi, T. High-molecular-weight AB-type benzoxazines as new precursors for high-performance thermosets. *J. Polym. Sci., Part A: Polym. Chem.* **2007**, *45*, 1878−1888.

https://doi.org/10.1021/acsomega.2c02067
ACS Omega 2022, 7, 26396−26406